

Part II. Free Surface Flow Simulation

In part I the fractional step method for the incompressible Navier-Stokes equations is applied to the free surface problem. However, for some reasons the steady solution cannot be obtained. In this part, following the recommendations made in part I, another numerical method to solve free surface problems using a fixed grid is described. The numerical scheme used here is the MAC method which is based on the basically same concept as the fractional step method to satisfy the divergence-free condition with pressure correction. The numerical results for the generation of periodic progressive wave are also shown.

5. Numerical Method

5.1 Governing Equations and Basic Algorithm

The governing equations are the two dimensional Navier-Stokes equations (2.1) and the continuity equation (2.2) for the incompressible fluid.

The general curvilinear coordinates system (ξ, η) is introduced to use the non-uniform grid. This computational coordinates do not fit to the free surface shape. The free surface configuration is determined by the nonlinear kinematic free surface condition. The coordinates transformation is given as follows;

$$\xi = \xi(x, y), \eta = \eta(x, y), t = t \quad (5.1)$$

The momentum equations (2.1) and the continuity equation (2.2) are transformed through equation (5.1) as;

$$\begin{aligned} & u_t + U u_\xi + V u_\eta \\ &= -(\xi_x p_\xi^* + \eta_x p_\eta^*) + \frac{1}{Re} (\nabla^2 u) \end{aligned} \quad (5.2a)$$

$$\begin{aligned} & v_t + U v_\xi + V v_\eta \\ &= -(\xi_y p_\xi^* + \eta_y p_\eta^*) + \frac{1}{Re} (\nabla^2 v) \end{aligned} \quad (5.2b)$$

$$\xi_x u_\xi + \eta_x u_\eta + \xi_y v_\xi + \eta_y v_\eta = 0 \quad (5.3)$$

where (U, V) are the unscaled contravariant velocity components and defined as

$$U = \xi_x u + \xi_y v \quad (5.4a)$$

$$V = \eta_x u + \eta_y v \quad (5.4b)$$

and p^* is modified pressure defined by equation (4.7)

∇^2 is the transformed Laplacian operator and defined as

$$\begin{aligned}\nabla^2 q &= (\xi_x^2 + \xi_y^2)q_{\xi\xi} + (\eta_x^2 + \eta_y^2)q_{\eta\eta} \\ &+ 2(\xi_x\eta_x + \xi_y\eta_y)q_{\xi\eta} \\ &+ (\xi_{xx} + \xi_{yy})q_\xi + (\eta_{xx} + \eta_{yy})q_\eta\end{aligned}\quad (5.5)$$

where q is arbitrary scalar quantity. ξ_x , ξ_y and so on appeared in equations (5.2)–(5.5) are the metrics of the grid. It should be noted that the transformed momentum equations (5.2) are not in the conservative form.

The basic algorithm is the same as that of the MAC method [9]. The discretization is made in the non-staggered grid, that is, all variables are defined in the intersections of grid lines. The present method is based on the time marching procedure and is divided into two stages.

On the first stage, velocity is updated by the momentum equations (5.2). The forward difference is used in time. The spatial differences are the fourth-order central difference for the convection terms and for the grid metrics terms and the second-order central difference for the pressure gradient terms. The fourth-derivative artificial numerical dissipation terms are added to the convection terms to stabilize computation. The resultant finite-difference equation for equation (5.2a) is

$$\begin{aligned}\frac{u_{i,j}^{n+1} - u_{i,j}}{\delta t} &= -U_{i,j} \frac{u_{i-2,j} - u_{i+2,j} - 8(u_{i-1,j} - u_{i+1,j})}{12} \\ &- \beta(u_{i-2,j} + u_{i+2,j} - 4(u_{i-1,j} + u_{i+1,j}) + 6u_{i,j}) \\ &- V_{i,j} \frac{u_{i,j-2} - u_{i,j+2} - 8(u_{i,j-1} - u_{i,j+1})}{12} \\ &- \beta(u_{i,j-2} + u_{i,j+2} - 4(u_{i,j-1} + u_{i,j+1}) + 6u_{i,j}) \\ &+ \frac{1}{Re} [(\xi_{xi,j}^2 + \xi_{yi,j}^2)(u_{i-1,j} - 2u_{i,j} + u_{i+1,j}) \\ &+ (\eta_{xi,j}^2 + \eta_{yi,j}^2)(u_{i,j-1} - 2u_{i,j} + u_{i,j+1}) \\ &+ 2(\xi_{xi,j}\eta_{xi,j} + \xi_{yi,j}\eta_{yi,j}) \frac{u_{i+1,j+1} - u_{i+1,j-1} - u_{i-1,j+1} + u_{i-1,j-1}}{4} \\ &+ (\xi_{xxi,j} + \xi_{yyi,j}) \frac{u_{i+1,j} - u_{i-1,j}}{2}\end{aligned}$$

$$\begin{aligned}
& +(\eta_{xxi,j} + \eta_{yyi,j}) \frac{u_{i,j+1} - u_{i,j-1}}{2} \\
& -\xi_{xi,j} \frac{p_{i+1,j}^* - p_{i-1,j}^*}{2} \\
& -\eta_{xi,j} \frac{p_{i,j+1}^* - p_{i,j-1}^*}{2}
\end{aligned} \tag{5.6}$$

where superscript $n + 1$ denotes the value at $(n + 1)$ -th step and superscripts n are dropped for simplicity. δt is the time increment and β is the parameter that determines the magnitude of the artificial dissipation.

On the second stage, pressure on the next time step is computed so that the velocity field on the next time step may satisfy the continuity condition. By taking divergence of the momentum equations (5.2), the following Poisson equation for pressure is derived.

$$\begin{aligned}
\nabla^2 p^* = & -\xi_x K_\xi - \eta_x K_\eta \\
& -\xi_y L_\xi - \eta_y L_\eta \\
& -D_t
\end{aligned} \tag{5.7}$$

where

$$K = U u_\xi + V u_\eta - \frac{1}{Re} (\nabla^2 u)$$

$$L = U v_\xi + V v_\eta - \frac{1}{Re} (\nabla^2 v)$$

$$D = \xi_x u_\xi + \eta_x u_\eta + \xi_y v_\xi + \eta_y v_\eta$$

The right-hand-side of equation (5.7) is evaluated by the values at the present time step. The spatial differences for K and L are the same as those for equation (5.6). The time differential appeared in the last term is expressed by the forward difference. Then D , divergence of velocity, on the next time step is set zero from the continuity condition, while D on the present time step which is not necessarily zero due to numerical error is evaluated by the second-order central difference. This can eliminate the accumulation of numerical error [9]. The left-hand-side of equation (5.7) is evaluated by the second-order central difference and is solved iteratively by the Successive Over Relaxation method.

5.2 Free Surface Conditions

In this computation, the effects of viscosity and surface tension to the free surface conditions are neglected for simplicity. Therefore, the free surface conditions consist of the following two conditions. One is the pressure condition that means that pressure on the free surface is equal to atmospheric one or to prescribed value. The other is the kinematic condition that tells the fluid particles on the free surface keep staying on it. Because the grid points are not on the free surface in the present grid system, it is not easy to satisfy the free surface conditions on the exact location of the free surface.

The pressure condition is implemented in the solution process for the Poisson equation for pressure. To give the boundary condition at the intermediate point between grid points, where the free surface is located, the 'irregular stars method' used in the SUMMAC method [12] is extended to the curvilinear coordinates system.

The kinematic condition is used to determine the free surface shape in the time marching process. The wave elevation is defined in the computational coordinates as

$$\eta = h(\xi, t) \quad (5.8)$$

The kinematic condition is written as

$$h_t + Uh_\xi - V = 0 \quad \text{on} \quad \eta = h \quad (5.9)$$

equation (5.9) is transformed into the finite-difference form in the same manner as that for the momentum equations (5.6). Velocity (U, V) on the free surface is extrapolated equally from the value at the adjacent lower grid points.

5.3 Other Boundary Conditions

The periodic boundary condition is used in the horizontal, x -, direction because the progressive periodic waves are considered. At the bottom of the computational domain, pressure and velocity are set equal to the values of the adjacent inner points.

6. Generation of Periodic Wave

To demonstrate the applicability of the method, the generation of the periodic progressive waves is numerically simulated. The proper initial and boundary conditions to generate periodic waves are discussed in this section.

The simplest initial condition is the still state, that is, velocity is zero and pressure is hydrostatic in the whole domain of computation. Alternative is to give an analytic solution of a periodic wave as the initial condition. In the latter case, the linear analytic solution for waves of infinitesimal amplitude is not adequate because

the linearized free surface condition of the theory is not consistent with the fully nonlinear free surface condition implemented in the numerical scheme. Analytic solutions for waves of finite amplitude such as Stokes theory can be used as the initial condition. The former condition, the still state, is used here for simplicity.

One way to generate waves is the oscillation of velocity and/or pressure in the inflow boundary[13]. This method simulates numerically a wave maker of a flap or piston type in an actual experimental tank. However, this approach cannot be adopted when the periodic condition is used in the horizontal direction, because the numerical wave maker generates waves which propagate in two, positive x - and negative x -, directions. In case that the periodic condition is not used in space, the wave propagating in the direction opposite to the computational domain does not affect the solution. However, with the periodic boundary condition, two waves propagating in the opposite directions affect each other and the solution differs from that for a single wave.

The other way is to give pressure distribution on a free surface. Periodic distribution of surface pressure that runs with the constant speed can generate the periodic progressive wave. This does not conflict with the periodic boundary condition of the scheme and is used here.

7. Numerical Results

7.1 Computational Conditions

Computational grid used is shown in Figure 9. The grid is orthogonal and consists of straight lines, though the present scheme can cope with the general curvilinear grid. The number of grid points is 51×51 and the computational domain is

$$0 \leq x \leq 1.02$$

$$-0.990668 \leq y \leq 0.2$$

The grid spacing in the horizontal direction is constant and 0.02, while that in the vertical direction is gradually varying from 0.01, the minimum value, to 0.10564, the maximum. The grid points are clustered near the free surface. The time increment δt is set 0.002 and the parameter β is set 0.1.

7.2 Results

The pressure distribution on the free surface is given by the following equation,

$$p^*(x, y, t) = gy + gw_a \cos(kx - \sigma t) \quad (5.10)$$

where (x, y) are the free surface location at time t and w_a is the amplitude of pressure oscillation defined with the dimension of water head. k is the wave number defined by the wave length λ as

$$k = \frac{2\pi}{\lambda}$$

and σ is the angular frequency of the wave. In the water waves, σ is related to the wave length by the following relationship,

$$\sigma = \sqrt{\frac{2\pi g}{\lambda}}$$

Here, the wave length λ of the generated wave is set 1.02 so that the computational domain in the horizontal direction is equal to one wave length and w_a is set 0.002. The velocity vector maps and the pressure distribution at various time steps are shown in Figure 10. The periodic wave is generated well. The pressure distribution beneath the free surface is smoothly connected to the pressure on the free surface. The velocity distributions show the approximately exponential decay in the depthwise direction. Figure 11 shows the time history of the wave elevation at $x = 0$. The wave amplitude becomes almost steady and nearly equal to 0.02 at $t = 8$. The computed wave amplitude is about ten times as large as w_a . Further investigation is required to explain the relation between w_a and the wave amplitude. The period of the computed wave is about 0.81 and is almost equal to that given in the surface pressure condition.

8. Conclusion

In part I, the fractional step method for incompressible fluid is presented together with some numerical results. The extension of the method to free surface problems are then made. The troubles encountered in the application of the method to free surface flow problem are discussed and finally some recommendations for computation of the free surface flow using the fractional step method are made.

In part II, the numerical method based on the MAC method is applied to free surface problems. The boundary and initial conditions for the generation of periodic progressive waves are discussed. The computational results show that the wave that has the pre-determined wave length and frequency can be generated by the proper boundary and initial conditions.

The fractional step method has the advantage of the exact conservation of mass because it assures that the divergence-free condition is satisfied at each time

step. The MAC method is simpler than the fractional method. However, the mass conservation is satisfied only indirectly through the Poisson equation for pressure. Therefore, for applications that require the strict conservation of mass the fractional step method is preferable, though more efforts should be made to apply the fractional step method to free surface problems.

Acknowledgements

The first author was supported as a Fellow of the Science and Technology Agency of Japan during this work. The author also expresses his gratitude to the CFD group at the Ship Research Institute and Mr. Hung Le of Stanford University for their valuable input.

References

- [1] Lee, C.H., Squires, K.D., Bertoglio, J.P., and Ferziger, J.H., "Study of Lagrangian Characteristic Times using Direct Numerical Simulation", Symposium on Turbulent Shear Flows, Toulouse, France, August 1987.
- [2] Moser, R.D., and Moin, P., "Direct Numerical Simulation of Curved Turbulent Channel Flow", Report TF-20, Department of Mechanical Engineering, Stanford University, Stanford, CA.
- [3] Kim, J. and Moin P., "Application of Fractional-Step Method to Incompressible Navier-Stokes Equations", J. Comp. Phys., Vol. 59, pp. 308-323, 1984.
- [4] Chorin, A.J., J. Comp. Phys., Vol. 2, 1967.
- [5] Peyret, R., and Taylor, T.D., "Computational Methods for Fluid Flow", Springer-Verlag, 1983.
- [6] Anderson, Tannehill, and Pletcher, "Computational Fluid Mechanics and Heat Transfer", McGraw-Hill, 1984.
- [7] Lilly, D.K., Mon. Weather Rev., Vol. 93, 1965.
- [8] Schreiber, R., Keller, H.B., J. Comp. Phys., Vol. 49, 1983.
- [9] Harlow, F.H., and Welch, J.E., Phys. Fluids, Vol. 8, 1965.
- [10] Hino, T., "Computation of a Free surface Flow around an Advancing Ship by the Navier-Stokes Equations", Pro. 5th Intern. Conf. Num. Ship Hydro., Hiroshima, Japan, September 1989.
- [11] Hirt, C.W., and Shannon, J.P., "Free-Surface Stress Conditions for Incompressible Flow Calculations", J. Comp. Phys., Vol. 2, pp. 403-411, 1968.

- [12] Chan, R.K.-C., and Street, R.L., "A Computer Study of Finite-Amplitude Water Waves", J. Comp. Phys., Vol. 6, 1970.
- [13] Hino, T., Miyata H. and Kajitani, H., "A Numerical Solution Method for Non-linear Shallow Water Waves (First Report)", J. Soc. Nav. Arch. Japan, Vol.153,pp. 1-12, 1983.

Appendix A

For the staggered grid the pressure nodes are located one-half of a grid cell from the boundaries. Because of this the cosine series used to represent the pressure must be manipulated before fast transforms may be used. A cosine series for the variable ϕ with N points is

$$\phi_i = \sum_{l=0}^{N-1} \hat{\phi}_l \cos \frac{\pi l}{N} \left(i + \frac{1}{2}\right)$$

$$i = 0, 1, \dots, N-1 \quad (A.1)$$

Multiplying (A.1) by $\cos(\pi l'(i + 1/2)/N)$ and summing over i gives

$$\sum_{i=0}^{N-1} \phi_i \cos \left(\frac{\pi l'}{N} \left(i + \frac{1}{2}\right)\right) =$$

$$\sum_{i=0}^{N-1} \sum_{l=0}^{N-1} \hat{\phi}_l \cos \left(\frac{\pi l}{N} \left(i + \frac{1}{2}\right)\right) \cos \left(\frac{\pi l'}{N} \left(i + \frac{1}{2}\right)\right)$$

$$= \sum_{l=0}^{N-1} \hat{\phi}_l \frac{1}{2} \sum_{i=0}^{N-1} \left[\cos \frac{\pi}{N} (l + l') \left(i + \frac{1}{2}\right) \right.$$

$$\left. + \cos \frac{\pi}{N} (l - l') \left(i + \frac{1}{2}\right) \right] \quad (A.2)$$

To simplify this make use of the fact that the following quantity

$$\sum_{i=0}^{N-1} \cos \frac{\pi}{N} \left(i + \frac{1}{2}\right) j$$

is equal to 0 if $j \neq 0$ and equal to N if $j = 0$. Therefore, for $l \neq l'$ A.2 is zero and for $l = l' \neq 0$:

$$\sum_{i=0}^{N-1} \cos \frac{\pi}{N} (l + l') \left(i + \frac{1}{2}\right) = 0$$

$$\sum_{i=0}^{N-1} \cos \frac{\pi}{N} (l - l') \left(i + \frac{1}{2}\right) = N$$

For $l = l' = 0$

$$\sum_{i=0}^{N-1} \left[\cos \frac{\pi}{N} (l + l') \left(i + \frac{1}{2}\right) + \cos \frac{\pi}{N} (l - l') \left(i + \frac{1}{2}\right) \right] = 2N$$

thus

$$\hat{\phi}_l = \frac{2}{N} \sum_{i=0}^{N-1} \phi_i \cos \frac{\pi l}{N} \left(i + \frac{1}{2}\right)$$

$$l = 0, 2, \dots, N - 1 \quad (A.3)$$

with a factor of $1/2$ multiplying the coefficient for $\hat{\phi}_0$. Equation (A.3) can be rewritten as

$$\begin{aligned} \hat{\phi}_l &= \frac{2}{N} \sum_{i=0}^{N-1} \phi_i \left[\cos \frac{\pi l i}{N} \cos \frac{\pi l}{2N} - \sin \frac{\pi l i}{N} \sin \frac{\pi l}{2N} \right] = \\ &= \frac{2}{N} \left(\sum_{i=0}^{N-1} \phi_i \cos \frac{\pi l i}{N} \right) \cos \frac{\pi l}{2N} - \frac{2}{N} \left(\sum_{i=0}^{N-1} \phi_i \sin \frac{\pi l i}{N} \right) \sin \frac{\pi l}{2N} \end{aligned} \quad (A.4)$$

Next consider the Fourier transform of the sequence of length $2N$

$$\begin{aligned} \phi_i &= \sum_{l=-\frac{2N}{2}}^{\frac{2N}{2}-1} \tilde{\phi}_l e^{i \frac{2\pi}{2N} l i} \\ i &= 0, 1, \dots, 2N - 1 \\ \tilde{\phi}_l &= \frac{1}{2N} \sum_{i=0}^{2N-1} \phi_i e^{-i \frac{2\pi}{2N} l i} \\ l &= -\frac{2N}{2}, \dots, 0, \dots, \frac{2N}{2} - 1 \end{aligned} \quad (A.5)$$

By choosing $\phi_i = 0$ for $i = N, N + 1, \dots, 2N - 1$ (A.5) becomes

$$\begin{aligned} \tilde{\phi}_l &= \frac{1}{2N} \sum_{i=0}^{N-1} \phi_i e^{-i \frac{\pi}{N} l i} \\ l &= -N, \dots, 0, \dots, N - 1 \end{aligned}$$

or

$$\begin{aligned} \tilde{\phi}_l &= \frac{1}{2N} \left[\left(\sum_{i=0}^{N-1} \phi_i \cos \frac{\pi l i}{N} \right) - i \left(\sum_{i=0}^{N-1} \phi_i \sin \frac{\pi l i}{N} \right) \right] \\ l &= -N, \dots, 0, \dots, N - 1 \end{aligned} \quad (A.6)$$

Comparing A.6 and A.4 gives

$$\begin{aligned} \hat{\phi}_l &= \frac{2}{N} \left[\text{Re}(\tilde{\phi}_l) \cos \frac{\pi l}{2N} + \text{Im}(\tilde{\phi}_l) \sin \frac{\pi l}{2N} \right] \\ l &= 0, 1, \dots, N - 1 \end{aligned} \quad (A.7)$$

Equation (A.7) gives the coefficients of the cosine series for the staggered grid. Similar manipulations are necessary for computing the function ϕ_i from the coefficients ϕ_l . The backward transform is given by:

$$\phi_i = \sum_{l=0}^{N-1} \hat{\phi}_l \cos \frac{\pi l}{N} \left(i + \frac{1}{2} \right)$$

$$i = 0, 1, \dots, N - 1 \quad (A.8)$$

Define the variable, ϕ_i^* as

$$\begin{aligned} \phi_i^* &= \sum_{l=0}^{N-1} \hat{\phi}_l e^{i\frac{\pi l}{N}(i+\frac{1}{2})} \\ &= \sum_{l=0}^{N-1} \hat{\phi}_l \cos \frac{\pi l}{N} (i + \frac{1}{2}) + i \sum_{l=0}^{N-1} \hat{\phi}_l \sin \frac{\pi l}{N} (i + \frac{1}{2}) \\ & \quad i = 0, 1, \dots, N - 1 \end{aligned} \quad (A.9)$$

Thus $\phi_i = \text{Re}(\phi_i^*)$

From (A.9)

$$\begin{aligned} \phi_i^* &= \sum_{l=-N}^{N-1} \hat{\phi}_l e^{i\frac{2\pi}{2N}l(i+\frac{1}{2})} \\ &= \sum_{l=-N}^{N-1} (\hat{\phi}_l \cos \frac{\pi l}{2N} + i \hat{\phi}_l \sin \frac{\pi l}{2N}) e^{i\frac{2\pi}{2N}li} \\ & \quad i = 0, 1, \dots, N - 1 \end{aligned}$$

if

$$\hat{\phi}_l = 0$$

for

$$l = -N, \dots, -1$$

Thus, to summarize:

- [1] Given a set of $\hat{\phi}_l$ (real), $l = 0, 1, \dots, N - 1$
- [2] Extend the sequence $\hat{\phi}_l$ to $2N$, $\hat{\phi}_l = 0$ for $l < 0$
- [3] Calculate $\tilde{\phi}_l = \hat{\phi}_l \cos \frac{\pi l}{2N} + i \hat{\phi}_l \sin \frac{\pi l}{2N}$
- [4] Backward transform $\tilde{\phi}_l, l = -N, \dots, 0, \dots, N - 1$ to obtain ϕ_i^*
- [5] ϕ_i will be the real part of ϕ_i^* .

Table 1 : Maximun error in the u velocity component after 30 steps.

Grid	Error
21×21	6.9724×10^{-5}
41×41	1.7588×10^{-5}

Table 2 : Stream function and vorticity at center of primary vortex for different Reynolds numbers.

Re	Present $\psi, (\omega)$ grid points	Kim and Moin [3] $\psi, (\omega)$ grid points	Schreiber and Keller [8] $\psi, (\omega)$ grid points
1	-0.100, (-3.217) 65 × 65	-0.099, (-3.316) 65 × 65	-0.100, (-3.232) 121 × 121
400	-0.112, (-2.257) 65 × 65	-0.112, (-2.260) 65 × 65	-0.113, (-2.281) 141 × 141
1000	-0.116, (-2.030) 97 × 97	-0.116, (-2.026) 97 × 97	-0.116, (-2.026) 141 × 141
4000	-0.112, (-1.804) 97 × 97	-0.114, (-1.879) 97 × 97	-0.112, (-1.805) 161 × 161

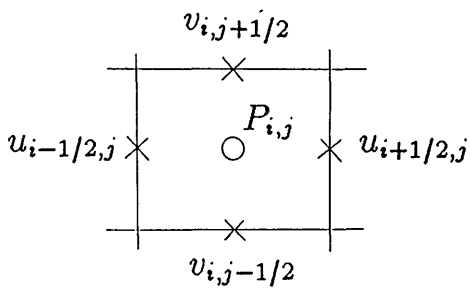


Fig. 1 Staggered grid in two dimensions.

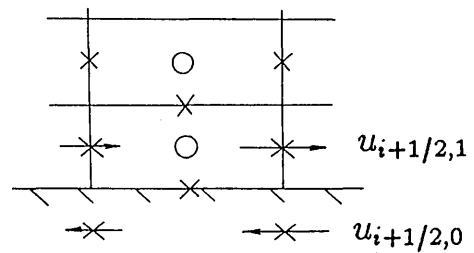
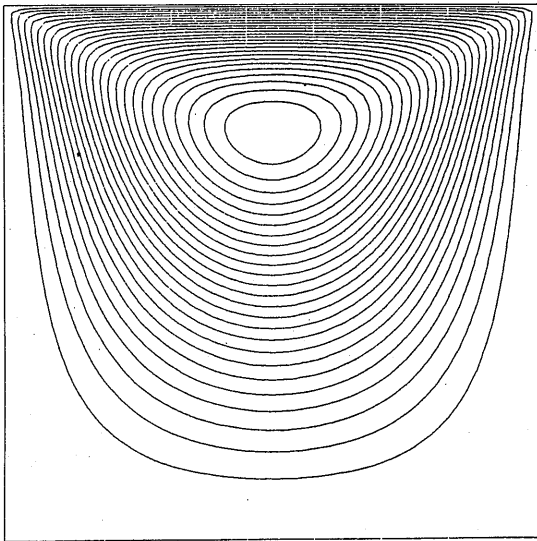
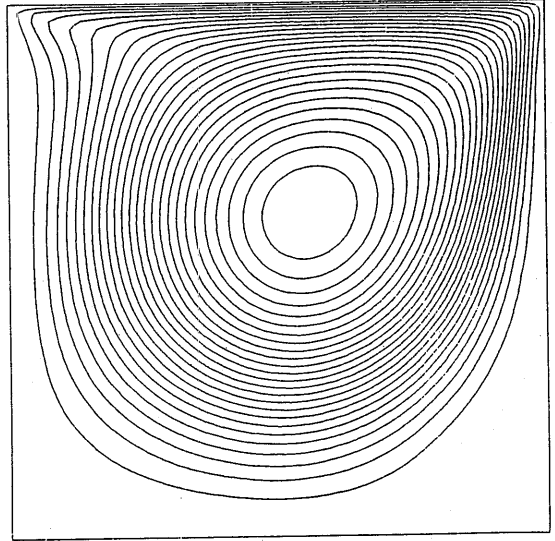


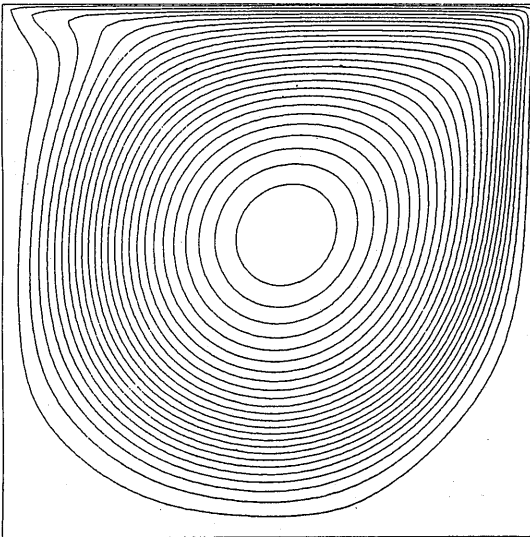
Fig. 2 Staggered grid near boundaries.



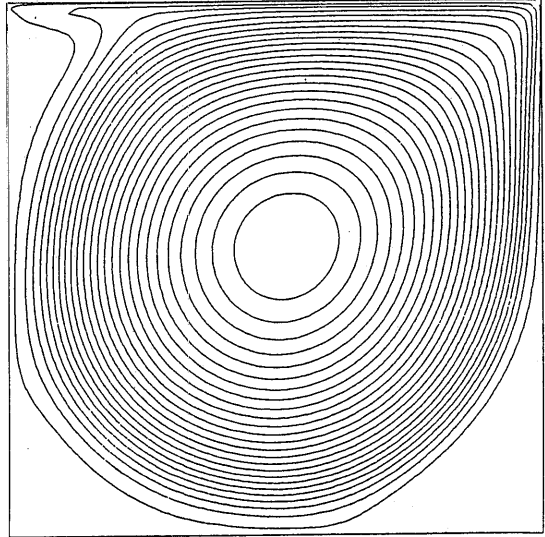
(a)



(b)

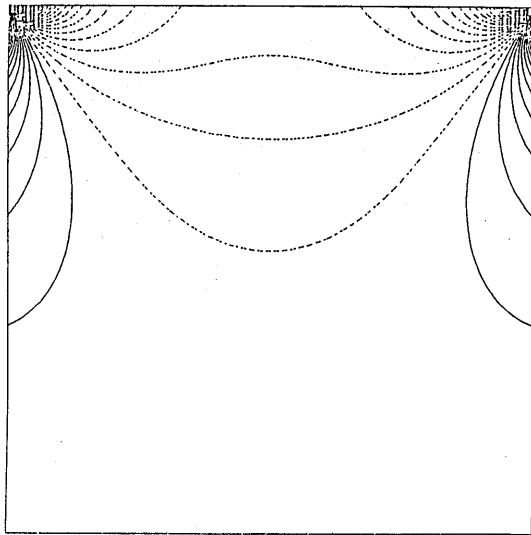


(c)

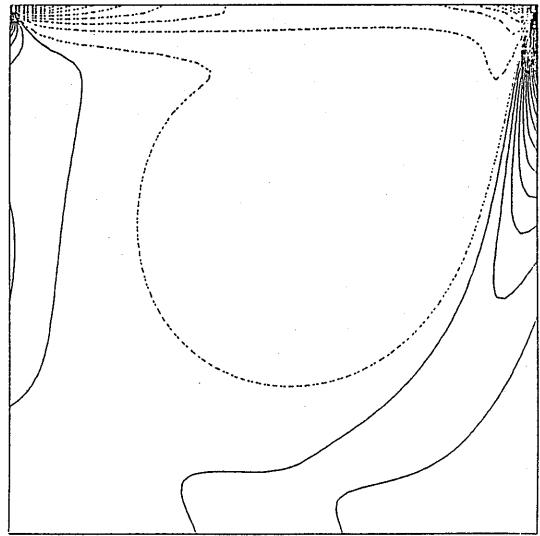


(d)

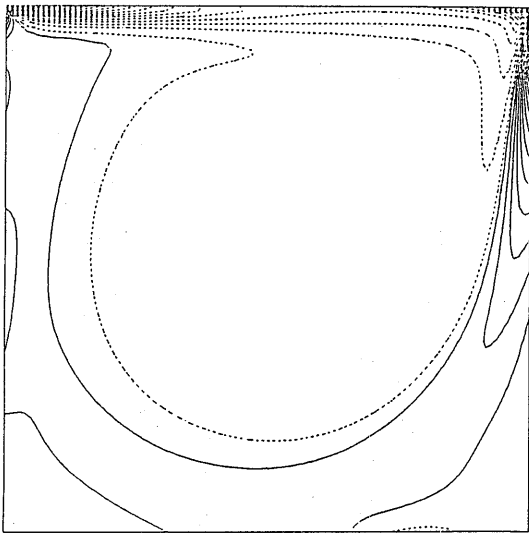
Fig. 3 Streamlines from cavity flow. (a) $Re=1$, (b) $Re=400$, (c) $Re=1000$, (d) $Re=4000$.



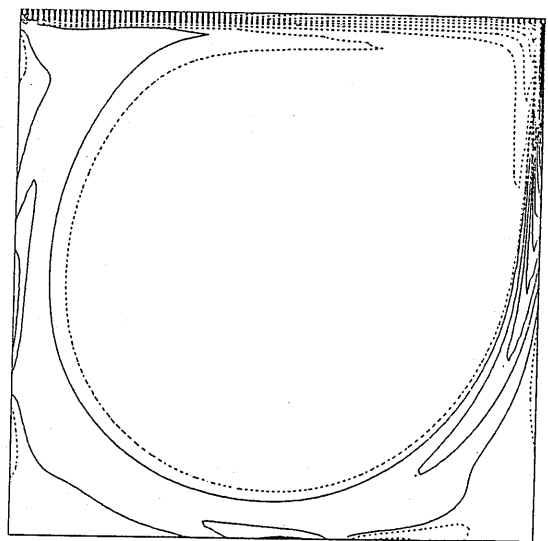
(a)



(b)



(c)



(d)

Fig. 4 Contours of constant vorticity from cavity flow. (a) $Re=1$, (b) $Re=400$,
(c) $Re=1000$, (d) $Re=4000$.

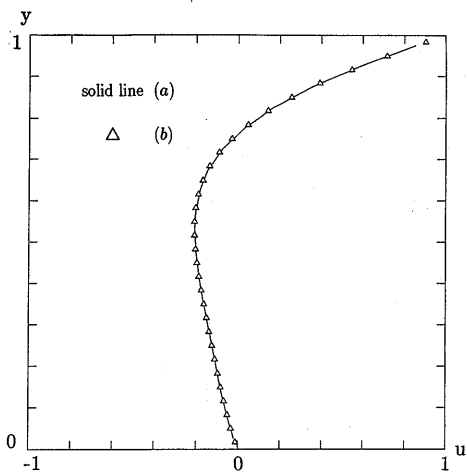


Fig. 5 Streamwise velocity profile at cavity midplane for $Re=1$. (a) 21×21 , (b) 31×31 .

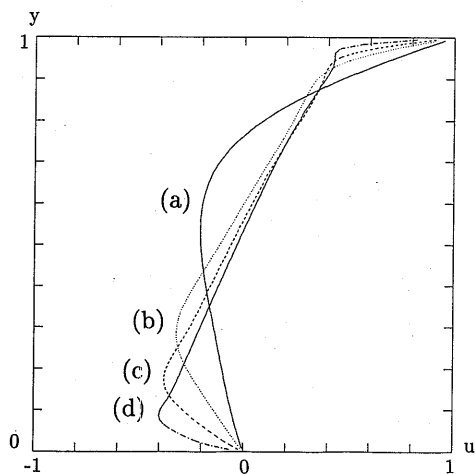


Fig. 7 Streamwise velocity profiles at cavity midplane for (a) $Re=1$, (b) $Re=400$, (c) $Re=1000$, (d) $Re=4000$.

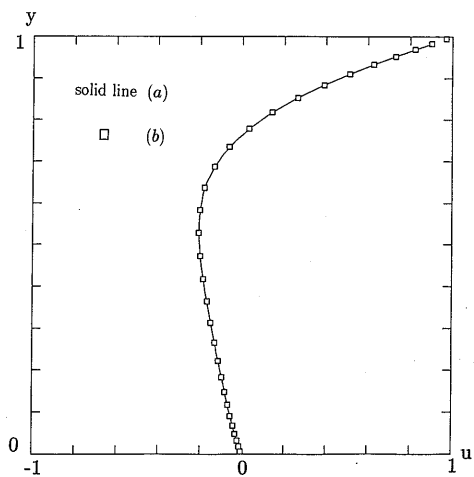


Fig. 6 Streamwise velocity profile at cavity midplane for $Re=1$, 31×31 . (a) uniform grid, (b) non-uniform grid.

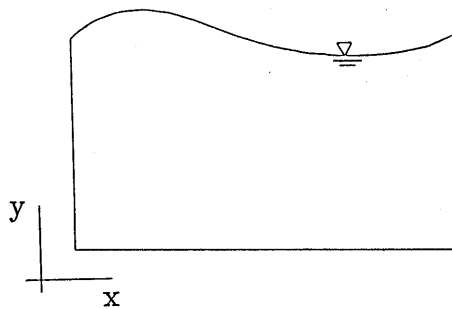


Fig. 8 Geometry of free surface flow.

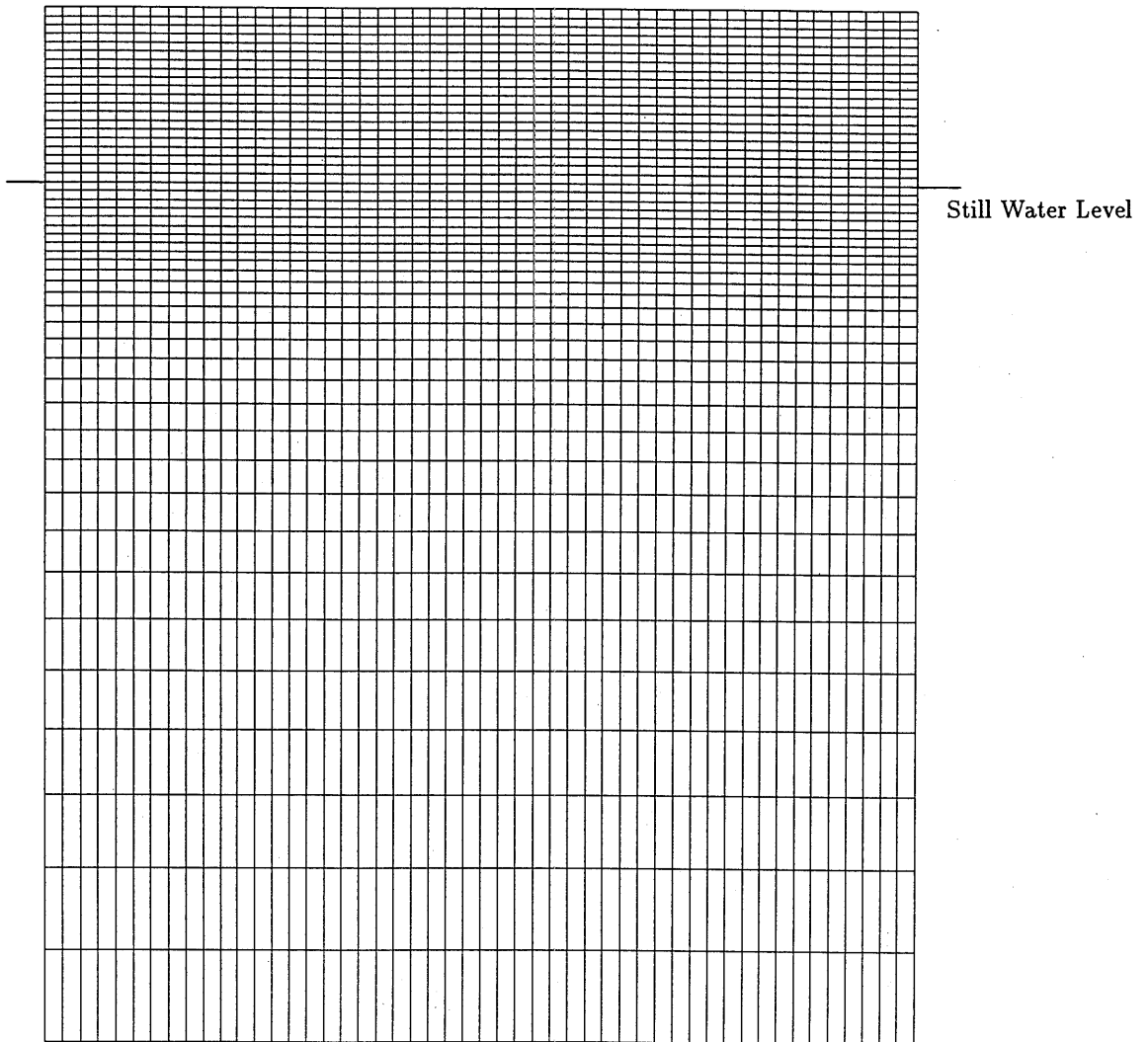


Fig. 9 Computaional grid for periodic wave generation.

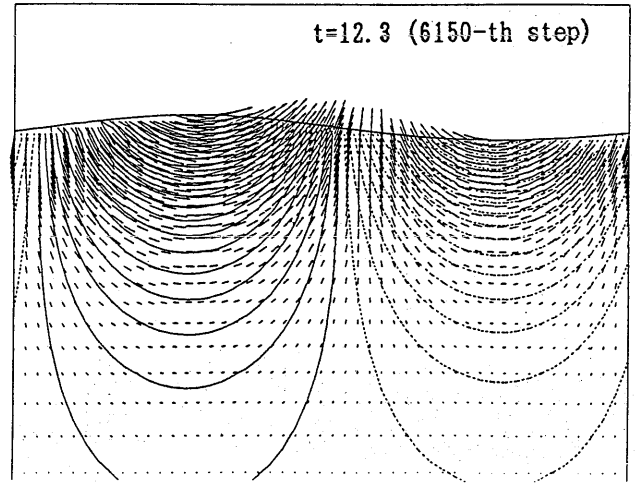
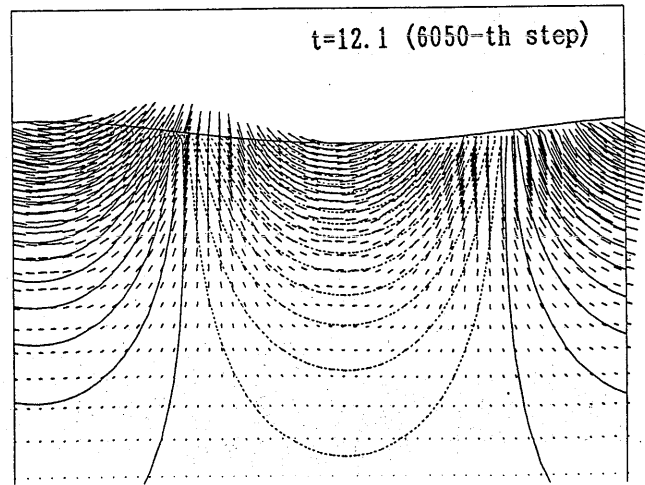
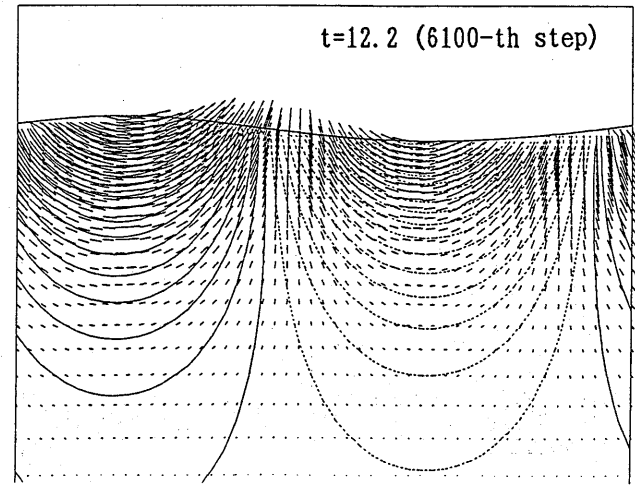
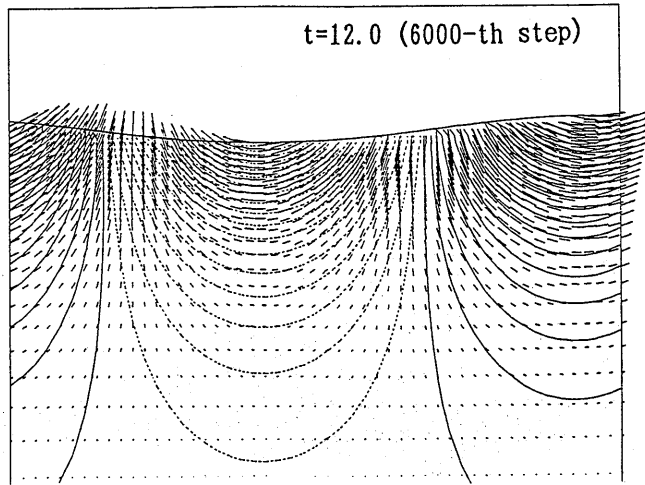


Fig. 10a Velocity vectors and pressure contours on various time steps.

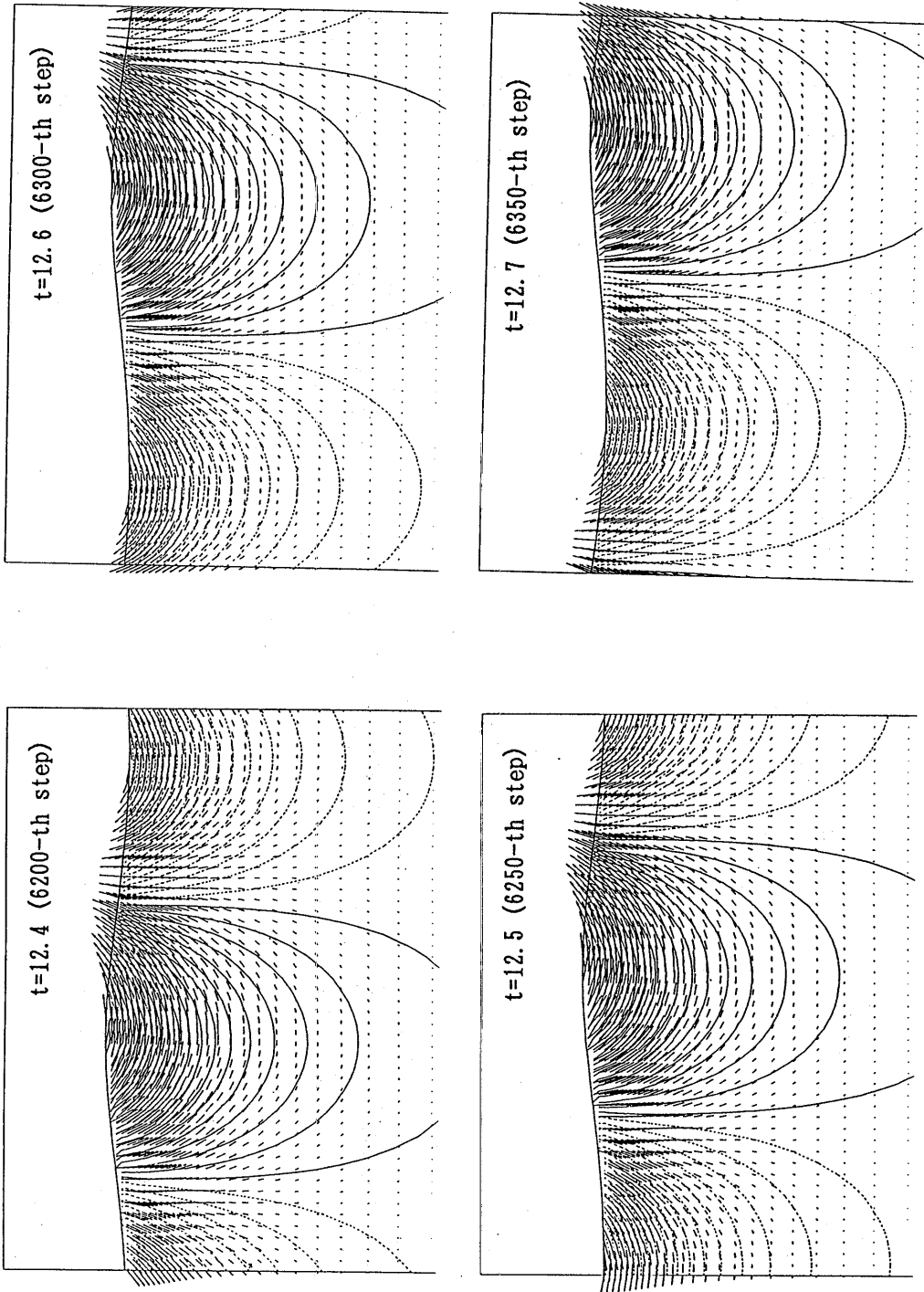


Fig. 10b (continued from Fig.10 a).

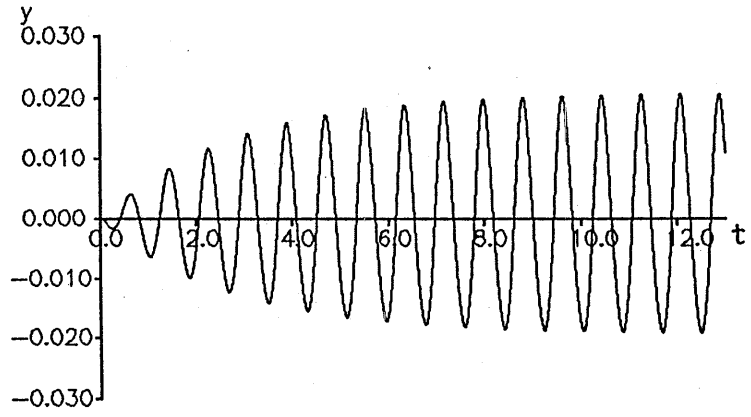


Fig. 11 Time history of wave elevation at $x=0$.